



UNIVERSITÀ
DEGLI STUDI
FIRENZE

FLORE

Repository istituzionale dell'Università degli Studi di Firenze

Evaluation of SCO1 deletion on *Saccharomyces cerevisiae* metabolism through a proteomic approach

Questa è la Versione finale referata (Post print/Accepted manuscript) della seguente pubblicazione:

Original Citation:

Evaluation of SCO1 deletion on *Saccharomyces cerevisiae* metabolism through a proteomic approach / Gamberi, T; Puglia, M; Bianchi, L; Gimigliano, A; Landi, C; Magherini, F; Guidi, F; Ranaldi, F; Armini, A; Cipriano, M; Gagliardi, A; Modesti, A; Bini, L. - In: PROTEOMICS. - ISSN 1615-9853. - ELETTRONICO. - 12:(2012), pp. 1767-1780. [10.1002/pmic.201100285]

Availability:

This version is available at: 2158/650640 since: 2016-01-12T16:59:29Z

Published version:

DOI: 10.1002/pmic.201100285

Terms of use:

Open Access

La pubblicazione è resa disponibile sotto le norme e i termini della licenza di deposito, secondo quanto stabilito dalla Policy per l'accesso aperto dell'Università degli Studi di Firenze (<https://www.sba.unifi.it/upload/policy-oa-2016-1.pdf>)

Publisher copyright claim:

(Article begins on next page)

RESEARCH ARTICLE

Evaluation of *SCO1* deletion on *Saccharomyces cerevisiae* metabolism through a proteomic approach

Tania Gamberi^{1*}, Michele Puglia^{2*}, Laura Bianchi², Anna Gimigliano², Claudia Landi², Francesca Magherini¹, Francesca Guidi¹, Francesco Ranaldi¹, Alessandro Armini², Maria Cipriano², Assunta Gagliardi², Alessandra Modesti^{1**} and Luca Bini²

¹ Department of Biochemical Sciences, University of Florence, Florence, Italy

² Department of Biotechnologies, University of Siena, Siena, Italy

The *Saccharomyces cerevisiae* gene *SCO1* has been shown to play an essential role in copper delivery to cytochrome *c* oxidase. Biochemical studies demonstrated specific transfer of copper from Cox1p to Sco1p, and physical interactions between the Sco1p and Cox2p. Deletion of *SCO1* yeast gene results in a respiratory deficient phenotype. This study aims to gain a more detailed insight on the effects of *SCO1* deletion on *S. cerevisiae* metabolism. We compared, using a proteomic approach, the protein pattern of *SCO1* null mutant strain and wild-type BY4741 strain grown on fermentable and on nonfermentable carbon sources. The analysis showed that on nonfermentable medium, the *SCO1* mutant displayed a protein profile similar to that of actively fermenting yeast cells. Indeed, on 3% glycerol, this mutant displayed an increase of some glycolytic and fermentative enzymes such as glyceraldehyde-3-phosphate dehydrogenase 1, enolase 2, pyruvate decarboxylase 1, and alcohol dehydrogenase 1. These data were supported by immunoblotting and enzyme activity assay. Moreover, the ethanol assay and the oxygen consumption measurement demonstrated a fermentative activity in *SCO1* mutant on respiratory medium. Our results suggest that on nonfermentable carbon source, the lack of Sco1p causes a metabolic shift from respiration to fermentation.

Received: May 27, 2011
Revised: January 30, 2012
Accepted: February 21, 2012

**Keywords:**

Cell biology / Fermentative metabolism / Respiratory metabolism / Sco1p deficiency / Yeast proteome

1 Introduction

Sco proteins (synthesis of cytochrome *c* oxidase [COX]) are evolutionarily conserved; members of the Sco-protein family have been found in eukaryotic as well as in prokaryotic organisms [1]. Both humans and yeast have two paralogous *SCO*-like genes, *SCO1* and *SCO2* [2], that code for mitochondrial metallochaperone proteins. These have an essential but poorly understood role in copper delivery to COX. In mammals, COX, the terminal enzyme of the mitochondrial respi-

ratory chain, is present in the inner mitochondrial membrane as a dimer with each monomer consisting of 13 subunits. Three subunits are encoded by mitochondrial DNA (*COX1*, *COX2*, and *COX3*) and the remaining ten are encoded by nuclear genome [3, 4]. Subunits Cox1p, Cox2p, and Cox3p form the catalytic core of the complex. The redox-active prosthetic groups are located within Cox1p (hemes *a* + *a*₃ and Cu_B-center) and Cox2p (binuclear Cu_A-center) [5]. The assembly of COX is a complex process that requires a large number of ancillary nuclear factors [6]. Numerous COX assembly genes have been identified by extensive study in yeast *Saccharomyces cerevisiae* [7, 8]. Many of these have human homologues, for example, *COX10*, *COX11*, *COX15*, *COX17*, *COX19*, *LRPPRC*, *OXA1*, *PET112*, *SCO1*, *SCO2*, and *SURF1*. Perhaps

Correspondence: Professor Luca Bini, Department of Biotechnologies, University of Siena, Via Fiorentina 1, 53100 Siena, Italy

E-mail: luca.bini@unisi.it

Fax: +39-0577-234903

Abbreviations: **SCD**, synthetic medium plus 2% glucose; **SCG**, synthetic medium plus 3% glycerol and 0.1% glucose; **TCA cycle**, citric acid cycle

*These authors contributed equally to this work.

**Additional corresponding author: Professor Alessandra Modesti, E-mail: modesti@scibio.unifi.it

the most thoroughly characterized aspect of COX assembly is mitochondrial copper delivery to the nascent holoenzyme complex and, in particular, copper delivery to the Cox2p subunit's Cu_A site. In eukaryotes, it has been found that proteins Cox17p, Sco1p, Sco2p, and Cox11p are necessary for copper insertion into Cu_A and Cu_B redox centers of Cox2p [6]. The first accessory factor to be identified in this pathway was yeast Cox17p, a small molecular weight protein that is located both in the cytoplasm and in the intermembrane space [9]. A high copy suppressor screen of yeast *COX17* null strain allowed the identification of yeast *SCO1* and *SCO2*, which show an identity of about 50% [10]. Further biochemical studies of yeast proteins demonstrated a specific transfer of copper from Cox17p to Sco1p [11] and physical interactions between both Sco proteins and Cox2p [12, 13]. Moreover, Sco2p is able to restore respiration in *COX17* null mutants, but not in *SCO1* mutants. Although these data suggest that both Sco proteins act downstream of Cox17p in copper delivery of COX [10], only the deletion of yeast *SCO1* gene results in a respiratory deficient phenotype. In line with these phenotypic observations, we recently reported the analysis of mitochondrial proteome patterns in yeast deletion mutants *SCO1* and *SCO2* which revealed that only lack of *SCO1* affects mitochondrial function and stability. We demonstrated that during growth on respiratory media, BY4741*sco1*-Δ yeast mutant cells exhibit a loss of mitochondrial membrane potential, a decrease in the number of functional mitochondria and a decrease in the expression level of many mitochondrial respiratory function proteins in comparison to wild-type BY4741 and BY4741*sco2*-Δ mutant strains. On the contrary, the *SCO2* null mutant strain showed a mitochondrial proteomic pattern similar to that of the wild-type strain [14]. At present, the role of Sco2p in yeast mitochondrial copper delivery to COX remains enigmatic. Unlike yeast cells, human cells require two functional Sco proteins to assure viability [15]. Mutations in either human *SCO1* or *SCO2* lead to severe, tissue-specific COX deficiencies owed to a failure in holoenzyme assembling. Despite their high degree of identity at the amino acid level (40%) [11], *SCO1* mutations are predominantly associated with fatal infantile hepatocerebralomyopathy [16], whereas mutations in *SCO2* result in fatal infantile cardioencephalomyopathy [17, 18]. Studies on immortalized fibroblasts from *SCO1* and *SCO2* patients suggest that Sco1p and Sco2p have essential, nonoverlapping but cooperative functions in the biogenesis of the Cu_A site [15, 19]. Yeast *SCO1* is equivalent to mammalian *SCO1*. Neither human Sco1p nor Sco2p is able to rescue the respiratory deficient phenotype of yeast *SCO1* null mutant. However, a chimera containing the N-terminal portion of yeast Sco1p fused to the C-terminal segment of human Sco1p is functional in yeast *SCO1* null mutant [19]. Although significant progress has been made in the characterization of Sco proteins, particularly in yeast, our current understanding of their exact role in COX assembly remains limited. In particular, it is not known why two closely related proteins are essential for mitochondrial function in humans but not in yeast, and how mutations in one or

the other human gene lead to different tissue-specific COX deficiencies associated with different clinical phenotypes.

The present study aims to gain more detailed insight on the effects of *SCO1* deletion and thus of COX deficiency on *S. cerevisiae* metabolism. The fact that respiration is not essential for yeast viability makes this organism an excellent model system for delineating the molecular mechanisms underlying COX assembly defects. In this regard, we analyzed the *SCO1* null mutant protein pattern comparing it to that of the wild-type strain during growth on both fermentable and nonfermentable carbon sources. By using two-dimensional gel electrophoresis (2-DE) and mass spectrometry, we found an increase in fermentative enzyme levels in *SCO1* null mutant strain on nonfermentable carbon source compared to wild-type strain. These findings were confirmed by both Western blot analysis and enzyme activity assay. Moreover, on respiratory growth conditions, *SCO1* null mutant cells displayed an ethanol productivity and oxygen consumption similar to that of fermentative yeast strains. These data suggest that, on nonfermentable carbon sources, yeast cells respond to Sco1p loss by reconfiguring their metabolism (from respiration to fermentation) probably to overcome the absence of a functional mitochondrial respiratory chain and to maintain ATP supplies.

2 Materials and methods

2.1 Yeast strains, media, and growth conditions

The *S. cerevisiae* strains used in this study were as follows: wild-type BY4741 (MATa; his3Δ1; leu2Δ0; met15Δ0; ura3Δ0, from Euroscarf) and BY4741*sco1*-Δ (MATa; his3Δ1; leu2Δ0; met15Δ0; ura3Δ0; YBR037c::kanMX4, from Euroscarf). Cells were cultured at 30°C in synthetic complete (SC) medium containing 0.67% (w/v) of yeast nitrogen base without amino acids (USbiological, USA) supplemented with complete amino acid dropout solution (USbiological, USA). Carbon sources were as follows: 2% (w/v) glucose (SCD); 3% (v/v) glycerol supplemented with 0.1% (w/v) glucose (SCG); 0.1% (w/v) glucose; 3% (v/v) glycerol.

2.2 Growth phenotypes

Yeast cells were picked from fresh colonies and grown at 30°C, to an optical density (OD_{600 nm}) of 1–2 in SC medium containing 2% glucose as carbon source. Cells were collected by centrifugation, washed with sterile water, and then diluted to 10⁶ cells/mL in SCD, in SCG, SC with 0.1% glucose or in SC with 3% glycerol fresh media, using flasks with a volume/medium ratio of 3:1. The growth curve was monitored for 24 h by measuring the turbidity of the culture at 600 nm (OD_{600nm}) with a spectrophotometer.

2.3 Sample preparation and 2DE

Yeast cells were picked, centrifuged, and washed as described above, but diluted to 10^4 cells/mL in SCD and to 10^5 cells/mL in SCG fresh media. To evaluate biological variation, five independent growth experiments were performed for wild-type BY4741 and BY4741*sco1-Δ* strains on SCD and on SCG media. Fifty OD_{600nm} of cells were collected by centrifugation at mid-logarithmic phase (after 24 h), washed twice with sterile water, and resuspended in 1 mL of RIPA lysis buffer (50 mM Tris-HCl, pH 7.5, 150 mM NaCl, 1% (v/v) Nonidet P-40, 2 mM EGTA, and 100 mM NaF) plus yeast protease inhibitors cocktail (Sigma Aldrich, St. Gallen, CH). Cells were broken with glass beads in a Fastprep instrument (Savant) and protein extracts were clarified by centrifugation at $8000 \times g$ for 10 min. Proteins were precipitated by adding five volumes of cold acetone (-20°C). After 2 h at -20°C , precipitates were recovered by centrifugation at $12\,000 \times g$ for 15 min, supernatants were discarded and pellets were washed once with cold acetone, dried in vacuum for 5 min, dissolved in a 2D-PAGE lysis buffer (8 M urea, 65 mM DTE, and 4% (w/v) CHAPS) and then centrifuged at $12\,000 \times g$ for 1 min at room temperature. The yeast extract samples obtained were separated by 2DE as previously described [20,21]. Isoelectric focusing was carried out on nonlinear wide-range immobilized pH gradients (IPGs; pH 3.0–10; 18-cm-long IPG strips; GE Healthcare, Uppsala, Sweden) and achieved using an Ettan IPGphor™ system (GE Healthcare). The sample load for analytical runs was 60 μg of total protein directly on 350 μL of lysis buffer and 0.2% carrier ampholyte. For MS-preparative gels analysis, 800 μg of total protein was loaded on both cathodic and anodic ends of the IPGphor Cup Loading Strip Holders (GE Healthcare). Runs were performed at 16°C , until a total of 80 000 V/h for analytical and 110 000 V/h for preparative gels were reached. Focused strips were equilibrated in 6 M urea, 2% (w/v) SDS, 2% (w/v) DTE, 30% (v/v) glycerol, and 0.05 M Tris-HCl pH 6.8 for 12 min and subsequently for 5 min in the same urea/SDS/Tris-HCl buffer solution where DTT was substituted with 2.5% iodoacetamide. The second dimension gels were carried out at 15°C on 9–16% polyacrylamide linear gradient gels (24 cm \times 20 cm \times 1.5 mm) at 17 W/gel constant Watt using an Ettan Dalt II system (GE Healthcare). Runs were performed until the dye front reached the bottom of the gel, in accordance with Hochstrasser et al. [22]. For analytical purposes, gels were stained with ammoniacal silver nitrate [23]. The exposure time for silver staining was optimized to avoid overexposure of some gels in comparison to others. MS-preparative gels were stained with SYPRO Ruby (Bio-rad headquarters, Hercules, CA, USA) according to the manufacturer's instructions.

2.4 Image analysis and statistics

Analytical gel images stained by silver nitrate were digitized using a Molecular Dynamics 300S laser densitometer (4000 \times

5000 pixel, 12 bits/pixel; Sunnyvale, CA, USA) while preparative gel images stained with SYPRO Ruby were digitized with a Typhoon 9400 laser densitometer (GE Healthcare). Two-dimensional image analysis was carried out using ImageMaster 2D Platinum software version 6.0 (GE Healthcare). Relative spot volumes calculated as %V (V single spot/ V total spots on a gel, where V is the integration of the OD over the spot area) were used for quantitative analyses in order to decrease experimental errors. The normalized spot volume was averaged and standard deviation was calculated. The analysis was performed comparing each gel obtained from one yeast strain (wild-type or *sco1-Δ* mutant) in one growth condition (SCD or SCG) with the other gels. Statistical analysis of protein spot variation was carried out with the two-tailed *t*-test of the Excel 2007 Microsoft Office software. Protein spot variation was considered significant if it showed a *p*-value <0.05 and at least a twofold change in relative volume %V. We assessed the false discovery rate (FDR) by the free software R (<http://www.r-project.org>).

2.5 Mass spectrometry protein identification

Protein identification was mainly carried out by peptide mass fingerprinting (PMF) on Ettan MALDI-TOF Pro mass spectrometer (GE Healthcare) as previously described [24,25]. The SYPRO Ruby stained gels were subjected to an automatic cutting by Ettan Spot Picker (GE Healthcare), destained in 2.5 mM ammonium bicarbonate and 50% ACN and finally dehydrated in ACN. They were then rehydrated in trypsin solution and in-gel protein digestion was performed by overnight incubation at 37°C . Each protein digest (0.75 μL) was spotted onto the MALDI target and allowed to air dry. Then 0.75 μL of matrix solution (saturated solution of CHCA in 50% (v/v) ACN and 0.5% (v/v) TFA) was applied to the sample which was then dried again. Mass spectra were acquired automatically using the Ettan MALDI Evaluation software (GE Healthcare). Spectra were internally calibrated using the autoproteolysis peptides of trypsin (842.51 and 2211.10 Da). PMF searching was carried out in NCBI nr and Swiss Prot databases using MASCOT (Matrix Science Ltd., London, UK, <http://www.matrixscience.com>). Taxonomy was limited to *S. cerevisiae*, a mass tolerance of 100 ppm was allowed and the number of accepted missed cleavage sites was set to one. Alkylation of cysteine by carbamidomethylation was considered a fixed modification, while oxidation of methionine was considered as a possible modification. The criteria used to accept identifications included the extent of sequence coverage, the number of matched peptides, and a probabilistic score. Tryptic digests that did not produce MALDI-TOF unambiguous identifications were subsequently subjected to peptide sequencing on a nanoscale LC-ESI/MS-MS, as described in detail by Meiring et al. [26]. All the analyses were carried out on an LC-MS system consisting of a PHOENIX 40 (ThermoQuest Hemel Hempstead, UK) and an LCQ DECA IonTrap mass spectrometer (Finnigan,

San Jose, CA, USA). The peptides, after a manual injection (5 μ L) in a six-port valve, were trapped in a C18 trapping column (20 mm \times 100 μ m ID \times 360 μ m OD, Nanoseparations, Nieuwkoop, the Netherlands) using a 100% solvent A (HPLC grade water + 0.1% (v/v) formic acid) under a flow rate of 5 μ L/min for 10 min. A linear gradient up to 60% solvent B (ACN + 0.1% (v/v) formic acid) for 30 min was used for analytical separation and, using a precolumn splitter restrictor, we obtained a column flow rate of 100–125 nL/min on a C18 analytical column (30 cm \times 50 μ m ID \times 360 μ m OD, Nanoseparations). Before the injection of the next sample, both the trapping and analytical column were equilibrated for 10 min in 100% solvent B and for 10 min in 100% solvent A. The ESI emitter, a gold-coated fused silica (5 cm \times 25 μ m ID \times 360 μ m OD, Nanoseparations) was heated to 195°C. A high voltage of 2 kV was applied for stable spray operation. The LC pump, the mass spectrometer as well as the automatic mass spectra acquisitions were controlled using the Xcalibur[™] 1.2 system software (Thermo). The MS/MS ions search was carried out in Swiss-Prot and NCBI nr databases using MASCOT. Taxonomy was limited to *S. cerevisiae*, peptide precursor charge was set to 2+ or 3+, mass tolerance of ± 1.2 Da for precursor peptide and ± 0.6 Da for fragment peptides was allowed, and the number of accepted missed cleavage sites was set to one. Alkylation of cysteine by carbamidomethylation was taken as a fixed modification, while oxidation and phosphorylation were considered as possible modifications. We consider significant peptides with individual ions scores ($-10 \times \log[P]$, where P is the probability that the observed match is a random event) that indicate identity ($p < 0.05$).

2.6 Cluster analysis

Cluster analysis was carried out using the EPCLUST tool for clustering and analysis of gene-expression data within Expression Profiler. This set of tools for microarray analysis was developed at the European Bioinformatics Institute (EBI) [27] and is available online (<http://www.ebi.ac.uk/EP/EP/EPCLUST/>). The data were clustered and visualized as linear correlation-based distance (Pearson, centered) and complete linkage (maximum distance).

2.7 Western blot analysis

Yeast cell growth conditions were the same as those of the 2DE experiments. Cells were lysed in ice-cold RIPA buffer plus protease inhibitors cocktail for yeast cells (Sigma). Samples (30 μ g) were separated by 12% SDS-PAGE and transferred onto PVDF membrane (Millipore). Western immunoblottings were performed by using: a monoclonal antibody (16G9) against yeast mitochondrial porin 1 (A-6449, Molecular Probes); a monoclonal antibody (22C5) against yeast cytosolic 3-phosphoglycerate kinase, PGK1 (A-6457, Molecular

Probes); rabbit polyclonal GAPDH-HRP conjugated antibodies (Abcam, Cambridge, UK) against yeast GAPDH. All antibodies were diluted 10 000-fold. The reaction was detected by chemiluminescence with an ECL kit (GE Healthcare). As loading control anti-actin antibodies (Santa Cruz, Heidelberg, Germany) were used. Western blot analysis was performed in triplicate and two-tailed nonpaired Student's *t*-test was calculated using ORIGIN 6.0 (Microcal Software, Inc.) to determine if the relative change in *sco1-Δ* mutant strain was statistically significant in comparison to the wt-BY4741 strain ($p < 0.05$).

2.8 Enzyme activity measurements

Yeast cell growth conditions were the same as those of the 2DE experiments. Cells were washed twice with sterile water and lysed in 1 mL of TEA buffer (100 mM Triethanolamine pH 7.6, 1 mM DTE) plus protease inhibitors cocktail for yeast cells (Sigma). Isocitrate lyase activity was determined by the method of Dixon and Kornberg as described by Giachetti et al. [28]. The assay mixture contained in 1 mL final volume consisted of 80 mM HEPES (pH 7.0), 6 mM MgCl₂, 4 mM phenylhydrazine. The reaction was started by adding substrate (4 mM D,L-isocitrate). Glyoxylate-phenylhydrazine ($\epsilon = 17 \text{ mM}^{-1} \text{ cm}^{-1}$) formation was followed at 30°C at 324 nm, using a UV-2100 spectrophotometer (Shimadzu, Columbia, MD, USA). Enolase activity was determined according to Bergmeyer [29], following the NADH oxidation at 340 nm, using a UV-2100 spectrophotometer (Shimadzu). The assay mixture contained in 1 mL final volume consisted of 80 mM triethanolamine (pH 7.6), 4 mM MgSO₄, 0.2 mM NADH, 2 mM ADP, 7 units pyruvate kinase, 10 units lactic dehydrogenase. The reaction was started by adding substrate (2 mM 2-phosphoglycerate). Two independent experiments were performed. A two-tailed nonpaired Student's *t*-test was performed using ORIGIN 6.0 (Microcal Software).

2.9 Analytical determination

For the ethanol, glycerol, and glucose assay, cells were cultured as described in the Section 2.2. Concerning the ethanol production and oxygen consumption, 1 mL of growth was harvested both at mid-exponential phase and after 24 h. The cleared supernatant was collected to estimate ethanol production using the alcohol-dehydrogenase/aldehyde-dehydrogenase method (EnzyPlus, Difco, Italy). Cells pellet was washed twice with cold water and suspended in respiration buffer (0.1 M K-Phthalate, pH 5.0) to an OD₆₀₀ of 1.7. Oxygen consumption was measured at 30°C using an oxygen electrode (Hansatech Instruments). Respiratory rates are expressed as nmol O₂ min⁻¹ per mg of cells (dry weight). Glycerol and glucose concentrations in the medium supernatant were determined every 2 h for 24 h using enzymatic combination kits (K-GCROL and K-GLUC,

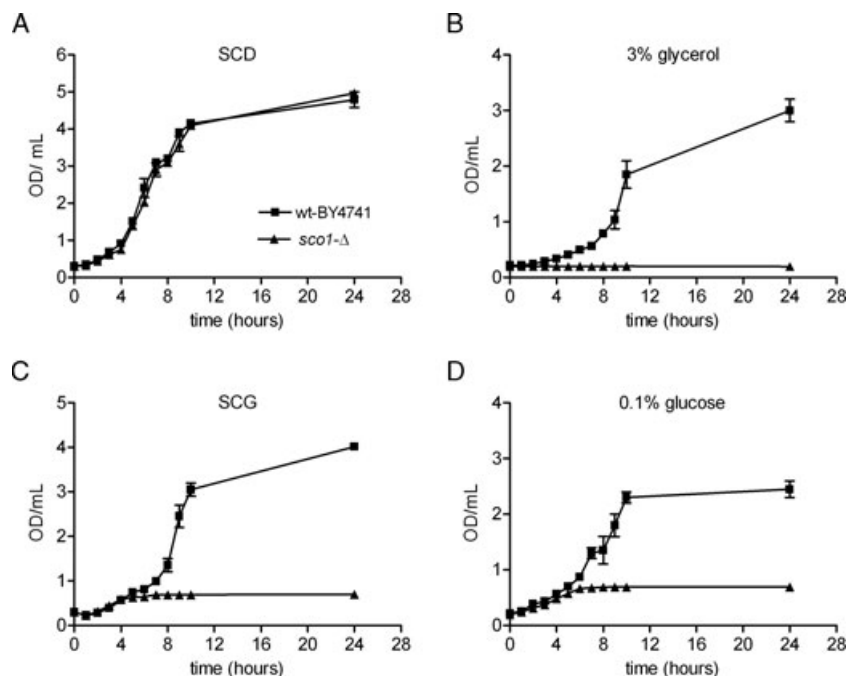


Figure 1. Growth curve of wt-BY4741 and BY4741 *sco1*-Δ mutant strain on 2% glucose (SCD) (A), on 3% glycerol (B), on 3% glycerol plus 0.1% glucose (SCG) (C), and on 0.1% glucose (D). Symbols: ■ BY4741 wild-type strain; ▲ BY4741 *sco1*-Δ mutant strain. Data represent mean and standard deviation obtained from three independent experiments.

from Megazyme, Wicklow, Ireland). Experiments were performed in triplicate. A two-tailed nonpaired Student's *t*-test was performed using ORIGIN 6.0 (Microcal Software).

2.10 Miscellaneous

Protein concentration was determined by standard Bradford method (Biorad).

3 Results

3.1 Growth phenotypes

Previous reports have shown that *SCO1* gene deletion affects yeast growth on respiratory carbon sources such as glycerol and ethanol. This growth defect is not detectable on fermentable media [10, 14, 30]. On medium containing 2% glucose (SCD), *sco1*-Δ mutant grew at a rate which was indistinguishable from that of the wild-type strain wt-BY4741 (Fig. 1A). Unlike the wild-type strain, *sco1*-Δ mutant was not able to grow on medium containing only 3% glycerol as carbon source (Fig. 1B). On the contrary, on 3% glycerol supplemented with 0.1% glucose (SCG), *sco1*-Δ mutant showed a decreased growth rate. In this condition, the *sco1*-Δ mutant strain duplicated only once in 24 h after which growth stopped (Fig. 1C). The SCG medium (5.5 mM of glucose concentration) is considered as nonfermentable since the amount of glucose required to switch metabolism from respiration to fermentation must be above 20 mM (approximately 0.4% (w/v)) [31, 32]. On medium containing 0.1% glucose as carbon

source, *sco1*-Δ mutant strain displayed a growth rate similar to that on SCG (Fig. 1D).

3.2 Proteomic analysis

In order to investigate differences between total protein expression in *S. cerevisiae* BY4741 wild-type strain and in *sco1*-Δ during mid-exponential growth on glucose or glycerol as carbon source, we performed a proteomic analysis by 2DE. In Fig. 2, representative 2DE images of soluble yeast proteins from wt-BY4741 (panel A) and *sco1*-Δ (panel B) grown on SCG, and from wt-BY4741 (panel C) and *sco1*-Δ (panel D) grown on SCD are reported. Approximately 1800 spots were detected in each silver-stained 2DE gel, representing a large subset of the high-abundant proteins in yeast. Spots ranged from 10 to 200 kDa and had a pH between 3 and 10. The gels showed a relatively similar protein pattern indicating the high degree of experimental reproducibility. The pattern and intensity of the spots present in all technical replicates proved a good overlapping to a 2DE reference gel for soluble yeast proteins available at <http://www.expasy.ch/swiss-2dpage/viewer>. The analysis was performed comparing each wild-type or *sco1*-Δ mutant proteomic profile both on SCD and on SCG. The results of these comparisons gave a total of 92 differentially expressed protein spots and 68 were identified by MS. The results of the MS identification as well as the relative amounts of these proteins are summarized in Table 1. To provide an overall reproducibility assessment of the proteomic analysis, we estimated the FDR. The results showed that an FDR ≤ 5% is associated to the differentially expressed protein spots (Supporting Information Table S1).

Table 1. Mass spectrometry identified proteins

Spot no. ^{a)}	AC ^{b)}	Protein name	Matched peptides ^{c)}	Sequence coverage ^{d)}	Score ^{e)}	% V ± SD		
						Wt-BY4741 SCD	Wt-BY4741 SCG	sco1-Δ SCG
Cluster 1								
1	P19882	Heat shock protein 60, mitochondrial	9	NVLEQPFPGPK	55	0.1031 ± 0.0574	0.0419 ± 0.0148	0.1163 ± 0.0366
2	P00925	Enolase 2	30		129	0.0731 ± 0.0564	0.0340 ± 0.0252	0.0718 ± 0.0418
3	P41277	(DL)-glycerol-3-phosphatase 1		VVVFEDAPAGIAAGK	56	0.0389 ± 0.0155	0.0193 ± 0.0113	0.0360 ± 0.0116
4	P06169	Pyruvate decarboxylase 1		TPANAAYPASTPLK	60	0.0837 ± 0.0365	0.0372 ± 0.0292	0.0743 ± 0.0298
5	P00925	Enolase 2	34		167	0.1120 ± 0.0554	0.0383 ± 0.0146	0.1111 ± 0.0372
6	P00560	Phosphoglycerate kinase		ELPGVAFLEK	51	0.0377 ± 0.0197	0.0187 ± 0.0057	0.0360 ± 0.0094
7	P38013	Peroxisomal type-2	68		146	1.0160 ± 0.1884	0.3252 ± 0.1547	0.9003 ± 0.2337
8	P29509	Thioredoxin reductase 1	44		151	0.2267 ± 0.1874	0.0704 ± 0.0565	0.1918 ± 0.1596
9	P14306	Carboxypeptidase Y inhibitor	41		106	0.0677 ± 0.0352	0.0256 ± 0.0052	0.0591 ± 0.0356
10	P00925	Enolase 2	32		131	0.1414 ± 0.0608	0.0718 ± 0.0434	0.1658 ± 0.0516
11	P38013	Peroxisomal type-2	43		119	0.2020 ± 0.0833	0.0629 ± 0.0230	0.2523 ± 0.1110
12	P00925	Enolase 2	32		114	0.3051 ± 0.1336	0.0537 ± 0.0367	0.3860 ± 0.2375
13	P00360	Glyceraldehyde-3-P dehydrogenase 1		TASGNIIPSTGAAG	50	0.0675 ± 0.0436	0.0247 ± 0.0114	0.1042 ± 0.0850
15	P38013	Peroxisomal type-2	51		87	0.2091 ± 0.0815	0.0461 ± 0.0179	0.3409 ± 0.1795
Cluster 2								
19	P02365	40S ribosomal protein S6		IGQVDGEAVGDEFK	47	0.1106 ± 0.0353	0.0541 ± 0.0462	0.0559 ± 0.0382
20	Q07953	SDO1-like protein	52		114	0.0848 ± 0.0320	0.0507 ± 0.0282	0.0693 ± 0.0490
21	P00445	Superoxide dismutase [Cu-Zn]	53		92	0.0516 ± 0.0215	0.0257 ± 0.0115	0.0485 ± 0.0274
22	P00925	Enolase 2	17		86	0.0773 ± 0.0241	0.0306 ± 0.0173	0.0836 ± 0.0388
24	P38013	Peroxisomal type-2	61		115	0.0732 ± 0.0238	0.0321 ± 0.0246	0.0783 ± 0.0233
25	P00445	Superoxide dismutase [Cu-Zn]		LIGTSTVVGR	37	0.0395 ± 0.0249	0.0137 ± 0.0071	0.0410 ± 0.0263
26	P00360	Glyceraldehyde-3-P dehydrogenase 1	28		90	0.1992 ± 0.1458	0.0565 ± 0.0582	0.2002 ± 0.0885
29	gi1181265	Pyruvate decarboxylase	34		67	0.1065 ± 0.0233	0.0475 ± 0.0229	0.1253 ± 0.0780
31	P38858	6-P gluconolactonase 3	50		201	0.1196 ± 0.0242	0.0503 ± 0.0206	0.0845 ± 0.0253
34	P22803	Thioredoxin-2		FAEQYSDAAFYK	67	0.1175 ± 0.0647	0.0000 ± 0.0000	0.0933 ± 0.0630
36	P34760	Peroxisomal type-2		FEEQGAQVLFASDTSEYSL	39	0.0551 ± 0.0177	0.0254 ± 0.0104	0.0370 ± 0.0096
				LAWTNIPR				
37	P13298	Orotate phosphoribosyltransferase 1		QEWSTDDKEGLSATQTVSK	47	0.1050 ± 0.0344	0.0164 ± 0.0228	0.0568 ± 0.0226
38	gi16322244	Cyt pr. involved in the reg. of enolase 1		VQGSYESLYDAGIMVR	89	0.0307 ± 0.0093	0.0073 ± 0.0038	0.0084 ± 0.0080
Cluster 3								
39	P38013	Peroxisomal type-2	63		126	0.0946 ± 0.0948	0.0612 ± 0.0274	0.1055 ± 0.0452
40	P00330	Alcohol dehydrogenase 1	36		139	0.1386 ± 0.0633	0.1052 ± 0.0619	0.1560 ± 0.0602
41	P00330	Alcohol dehydrogenase 1	26		101	0.0336 ± 0.0152	0.0240 ± 0.0252	0.0426 ± 0.0265
42	P28272	Dihydroorotate dehydrogenase		GYTSIDQFR	50	0.0969 ± 0.0568	0.0772 ± 0.0232	0.1059 ± 0.0410
43	P16140	V-type proton ATPase subunit B	23		115	0.0160 ± 0.0101	0.0189 ± 0.0095	0.0219 ± 0.0066
44	P38011	Guanine nucleotid-bind prot subunit B		ADDDSVTIIISAGNDK	72	0.0373 ± 0.0138	0.0365 ± 0.0224	0.0443 ± 0.0053
45	P06168	Ketol-acid reductoisomerase, mit.	26		112	0.0479 ± 0.0224	0.0478 ± 0.0201	0.0493 ± 0.0428
47	P12709	Glucose-6-phosphate isomerase	21		140	0.0251 ± 0.0255	0.0374 ± 0.0344	0.0454 ± 0.0302
48	P31373	Cystationine gamma-lyase		ISVGIEDTDLLEDIK	66	0.0000 ± 0.0000	0.0147 ± 0.0102	0.0201 ± 0.0194
49	P00330	Alcohol dehydrogenase 1	33		135	0.0867 ± 0.0413	0.0734 ± 0.0509	0.0532 ± 0.0242

Table 1. Continued

Spot no. ^{a)}	AC ^{b)}	Protein name	Matched peptides ^{c)}	Sequence coverage ^{d)}	Score ^{e)}	% V ± SD			
						Wt-BY4741 SCD	Wt-BY4741 SCG	sco1-Δ SCD	sco1-Δ SCG
Cluster 4									
51	P38625	GMP synthase [glutamine-hydrolyzing]	8	16	100	0.0158 ± 0.0082	0.0344 ± 0.0319	0.0280 ± 0.0226	0.0374 ± 0.0160
52	Q12230	Sphingolip. long ch. base-responsive protein	6	22	84	0.0311 ± 0.0149	0.0809 ± 0.0362	0.0445 ± 0.0251	0.1006 ± 0.0494
53	P04806	Hexokinase-1	10	27	133	0.0210 ± 0.0100	0.1113 ± 0.0776	0.0406 ± 0.0087	0.1207 ± 0.0390
56	P32891	D-lactate dehydrogenase1 [cytochrome]	EYLLLEGEAPVDLMR	48	48	0.0000 ± 0.0000	0.0169 ± 0.0079	0.0000 ± 0.0000	0.0342 ± 0.0329
58	P04806	Hexokinase-1	11	35	111	0.0359 ± 0.0277	0.1131 ± 0.0546	0.0246 ± 0.0149	0.0849 ± 0.0391
59	P00331	Alcohol dehydrogenase 2	7	26	117	0.0000 ± 0.0000	0.1574 ± 0.0765	0.0000 ± 0.0000	0.1357 ± 0.1669
60	P46367	K-activated aldehyde dehydro. mit.	9	28	121	0.0000 ± 0.0000	0.1333 ± 0.1215	0.0000 ± 0.0000	0.1098 ± 0.0472
64	P34730	Protein BMH2	6	32	100	0.0727 ± 0.0372	0.1486 ± 0.0655	0.0734 ± 0.0343	0.0952 ± 0.0507
65	Q00764	Alpha.alpha-trehalose-phospho synthase	9	23	118	0.0117 ± 0.0209	0.0718 ± 0.0443	0.0140 ± 0.0120	0.0325 ± 0.0160
66	P04806	Hexokinase-1	13	34	181	0.0283 ± 0.0222	0.1201 ± 0.0891	0.0314 ± 0.0103	0.0708 ± 0.0534
67	P10591	Heat shock protein SSA1	12	21	140	0.0000 ± 0.0000	0.0377 ± 0.0196	0.0000 ± 0.0000	0.0151 ± 0.0192
Cluster 5									
68	P04840	Mit. outer memb. protein porin 1	7	35	123	0.3640 ± 0.1299	0.4689 ± 0.0678	0.3160 ± 0.1195	0.1550 ± 0.0357
70	P25373	Glutaredoxin-1	6	70	106	0.0872 ± 0.0691	0.1135 ± 0.0131	0.0552 ± 0.0341	0.0408 ± 0.0280
72	P04037	Cytochrome oxidase subunit 4	EGTPTDLDQETGLAR	44	44	0.1031 ± 0.0313	0.1820 ± 0.0329	0.0515 ± 0.0449	0.0468 ± 0.0140
73	P01095	Protease B inhibitors 2. 1	5	70	110	0.1594 ± 0.0787	0.4032 ± 0.1469	0.2359 ± 0.1991	0.1527 ± 0.0556
74	P00924	Enolase 1	10	32	142	0.0401 ± 0.0276	0.1142 ± 0.0561	0.0616 ± 0.0226	0.0575 ± 0.0195
75	Q12363	Transcriptional modulator	8	23	108	0.0127 ± 0.0109	0.0760 ± 0.0379	0.0214 ± 0.0126	0.0228 ± 0.0165
76	P53312	Succ-CoA ligase [ADP-forming] sub. beta	8	29	97	0.0000 ± 0.0000	0.0401 ± 0.0240	0.0080 ± 0.0061	0.0081 ± 0.0086
77	P17505	Malate dehydrogenase	17	60	225	0.1511 ± 0.1304	0.3283 ± 0.0534	0.0617 ± 0.0179	0.1260 ± 0.0776
78	P00427	Cytochrome oxidase subunit 6	7	54	121	0.0165 ± 0.0114	0.0896 ± 0.0331	0.0000 ± 0.0000	0.0201 ± 0.0171
79	P19262	Component of 2-oxoglut. dehy complex	5	14	79	0.0291 ± 0.0234	0.1514 ± 0.1021	0.0206 ± 0.0144	0.0393 ± 0.0196
80	P00830	ATP synthase subunit beta	16	39	206	0.0408 ± 0.0182	0.1700 ± 0.0696	0.0382 ± 0.0246	0.0443 ± 0.0260
81	P28240	Isocitrate lyase	11	25	165	0.0047 ± 0.0021	0.0194 ± 0.0092	0.0038 ± 0.0018	0.0052 ± 0.0041
83	P00830	ATP synthase subunit beta	17	43	177	0.1622 ± 0.0749	0.4906 ± 0.2578	0.0987 ± 0.0656	0.1240 ± 0.0537
84	P00942	Triosephosphate isomerase	ILYGGSGANGSNAVTFK	46	46	0.0274 ± 0.0116	0.0610 ± 0.0276	0.0191 ± 0.0066	0.0163 ± 0.0039
86	gi 9755343	Putative pr.; exp is reg. by Msn2p/Msn4p	5	69	119	0.0118 ± 0.0128	0.0752 ± 0.0470	0.0000 ± 0.0000	0.0000 ± 0.0000
87	P07251	ATP synthase subunit alpha	14	36	204	0.0184 ± 0.0119	0.0901 ± 0.0691	0.0213 ± 0.0244	0.0069 ± 0.0085
88	P34227	Mitochondrial peroxiredoxin	VIDALQLTDK	39	58	0.0543 ± 0.0368	0.1161 ± 0.0542	0.0578 ± 0.0287	0.0540 ± 0.0126
90	P09457	ATP synthase subunit 5	6	39	75	0.0005 ± 0.0011	0.0204 ± 0.0139	0.0000 ± 0.0000	0.0000 ± 0.0000
91	P19262	Component of 2-oxoglut. dehy complex	AQEPVVASNSFTPFPR	74	74	0.0000 ± 0.0000	0.1033 ± 0.0276	0.0000 ± 0.0000	0.0000 ± 0.0000
92	P41940	Mannose 1 phosphate	7	29	83	0.0000 ± 0.0000	0.0171 ± 0.0116	0.0000 ± 0.0000	0.0000 ± 0.0000

Reported sequence peptide corresponds to one of those resulted from MS/MS analysis after ambiguous identifications by MALDI-TOF in that spot.
a) Spot number match those reported in the representative 2D silver-stained gels shown in Fig. 2.

b) Accession number in SwissProt/Tremble or NCBItr.

c) Number of matched peptides correspond to peptide masses matching the top hit from Ms-Fit PMF.

d) Sequence coverage percent indicates (number of the identified residues/total number of amino acid residues in the protein sequence) × 100.

e) Score corresponds to MASCOT score (Matrix Science, London, UK; <http://www.matrixscience.com>).

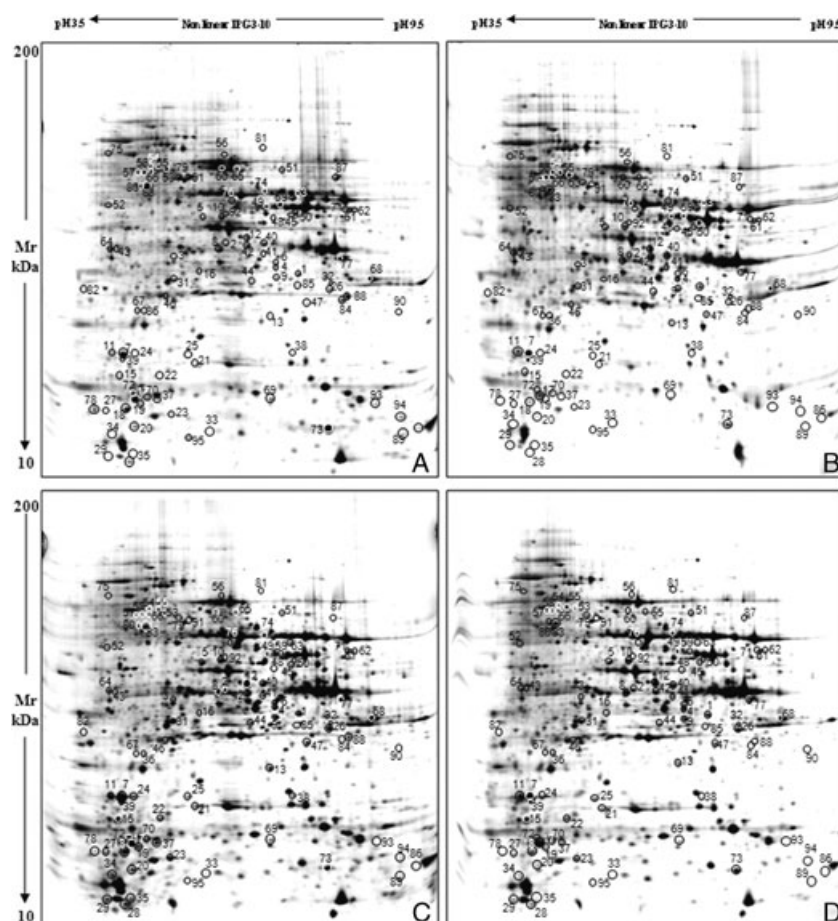


Figure 2. Representative 2D silver-stained gels of total protein extract from wt-BY4741 (A) and *sco1*- Δ mutant strain (B) grown in SCG, and from wt-BY4741 (C), and *sco1*- Δ (D) grown in SCD. Black and white circles with numbers visualize quantitative and qualitative differences found among the electropherograms.

3.3 Cluster analysis and identification of differentially expressed proteins

To investigate how the two different types of carbon sources affect the expression levels of specific proteins in wt-BY4741 and *sco1*- Δ , we decided to perform a cluster analysis to highlight proteins with similar expression patterns. The clusterization allowed us to classify the 92 variations in different clusters of proteins whose expression level followed the same trend. Five major clusters were obtained (Fig. 3). In Table 1, the cluster subdivision of the 68 proteins identified by MS as well as their relative amounts and biological functions were reported.

3.3.1 Cluster 1

It includes a total of 16 protein spots whose expression level increased in wt-BY4741, in *sco1*- Δ strains grown on SCD and in *sco1*- Δ strain grown on SCG. Among them, 14 were identified by MS. As shown in Table 1, we identified some glycolytic enzymes such as enolase 2 (Spots 2, 5, 10, and 12), 3-phosphoglycerate kinase (Spot 6), glyceraldehyde-3-phosphate dehydrogenase 1 (GAPDH) (Spot 13). Concern-

ing fermentation, we found pyruvate decarboxylase isozyme 1 (Spot 4) and an enzyme involved in glycerol biosynthesis: glycerol-3-phosphatase 1 (Spot 3). We also identified a group of stress response proteins: heat shock protein Hsp60p (Spot 1), peroxiredoxin type-2 (Spots 7, 11, and 15), and thioredoxin reductase 1 (Spot 8). Finally, we identified carboxypeptidase Y inhibitor (Spot 9).

3.3.2 Cluster 2

It includes a total of 21 protein spots whose expression is correlated with the carbon source and not with *SCO1* gene deletion. During growth on SCD, these proteins resulted over-expressed in both strains in comparison to growth on SCG. Twelve proteins were successfully identified by MS. As shown in Table 1, these proteins belong to glycolytic and fermentative pathways such as enolase 2 (Spot 22), glyceraldehyde-3-phosphate dehydrogenase (Spot 26), and pyruvate decarboxylase isozyme 1 (Spot 29). We found a protein involved in the pentose phosphate pathway, 6-phosphogluconolactonase (Spot 31), and an enzyme belonging to the uracil biosynthesis pathway: orotate phosphoribosyltransferase 1 (Spot 37). We also identified a group of stress response proteins such as

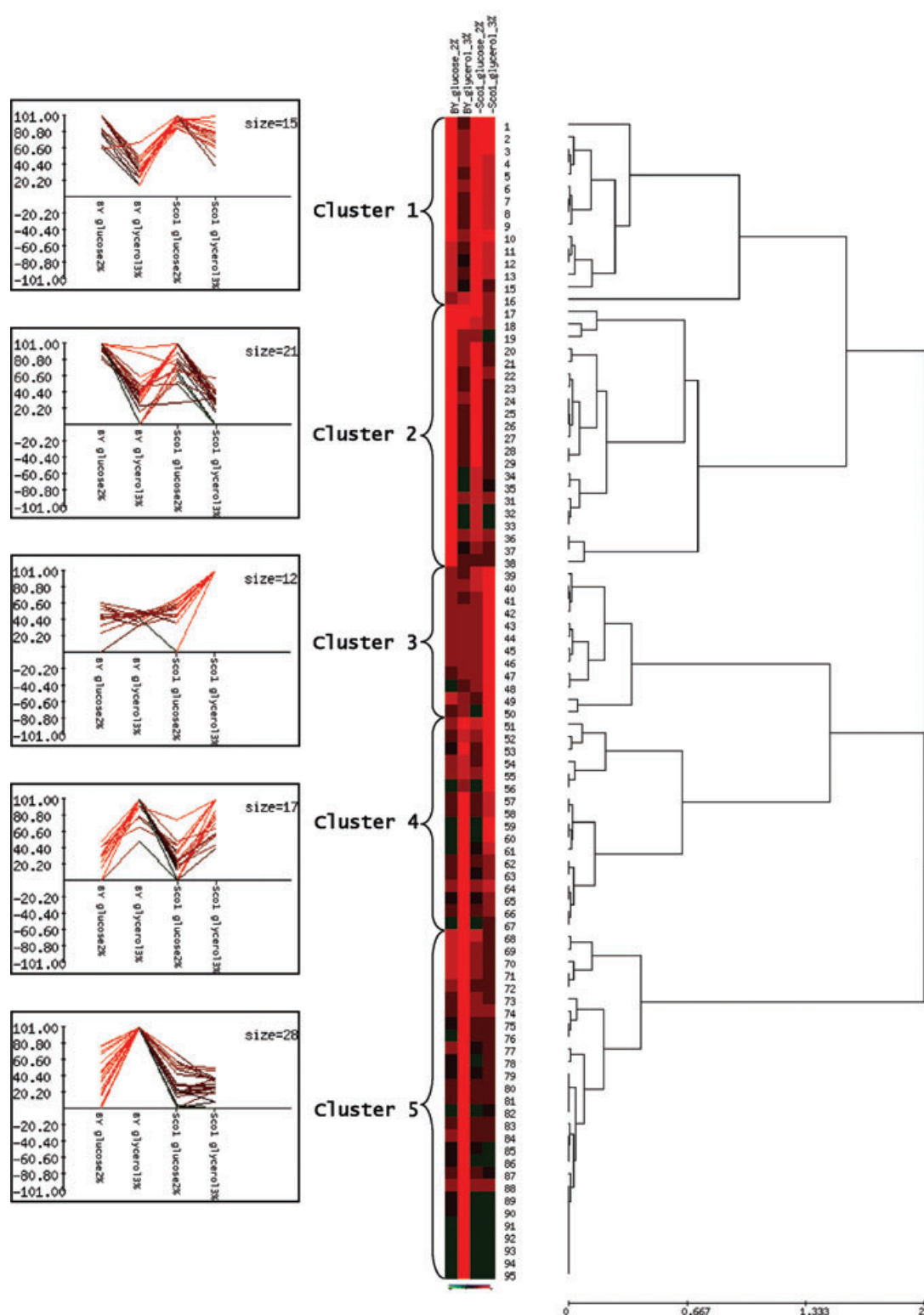


Figure 3. Cluster analysis of differentially expressed proteins in wild-type and *sco1*-Δ mutant strains during growth in SCD and SCG. (Right) Normalized %V mean values of differences obtained by %V values individually computed in the yeast strains wt-BY4741 and *sco1*-Δ mutant. Each reported value is proportional to the intensity of the color and its corresponding spot number is annotated on the right of the diagram near the complete linkage clustering based on Pearson distance. The major clusters are numbered from top to bottom. (Left) Normalized %V mean values of the four tested conditions clustered in five main groups. Cluster number and size are reported. The color saturation indicates the magnitude of relative spot level (black = 0 and red = 100).

peroxiredoxin type-2 (Spot 24) and peroxiredoxin 1 (Spot 36), thioredoxin-2 (Spot 34), and cytosolic superoxide dismutase (Spots 21 and 25). Finally, we identified two protein spots associated with ribosome assembly: 40S ribosomal protein S6 (Spot 19) and 60S ribosome maturation factor (Spot 20).

3.3.3 Cluster 3

It includes 12 protein spots that have the common trend to increase their expression level only when *sco1*-Δ strain is grown on SCG. We identified ten proteins by MS (Table 1). Three of them correspond to alcohol dehydrogenase 1 (Spots 40, 41, and 49). We identified the glycolytic enzyme glucose-6-phosphate isomerase (Spot 47) and three proteins involved in amino acid metabolism: ketol-acid reductoisomerase (Spot 45), cystationine gamma-lyase (Spot 48), and dihydroorotate dehydrogenase (Spot 42). Finally, we identified Asc1p, the G-protein beta subunit of Gpa2p (Spot 44).

3.3.4 Cluster 4

It includes 17 proteins showing an opposite expression trend in comparison to the Cluster 2. These proteins resulted up-regulated in both wt-BY4741 and in *sco1*-Δ strains grown on SCG. Twelve proteins have been successfully identified (Table 1). Most of these proteins are involved in energy and carbohydrate metabolism: hexokinase isoenzyme 1 (Spot 53, 58, and 66), the glucose-repressible alcohol dehydrogenase 2 (Spot 59), and the mitochondrial aldehyde dehydrogenase 4 (Spot 60). We also identified the D-lactate dehydrogenase (Spot 56).

3.3.5 Cluster 5

It is a group of 28 protein spots showing an opposite trend in comparison to that of Cluster 1. The expression level of these protein spots increased in wt-BY4741 strain on SCG. We identified 20 proteins by MS. Most of these are mitochondrial proteins involved in the respiratory chain, for example, two subunits of COX: subunit 4 (Spot 72) and subunit 6 (Spot 78) and the ATP synthase complex (Spots 80, 83, 87, and 90), while others are involved in the citric acid cycle (TCA) and in metabolite and protein import across the mitochondrial membrane. TCA cycle enzymes include: the beta subunit of succinyl-CoA ligase (Spot 76); the mitochondrial malate dehydrogenase (Spot 77), and the mitochondrial dihydrolipoyl transsuccinylase (Spots 79 and 91) component of the 2-oxoglutarate dehydrogenase complex. We also identified a key enzyme of the glyoxylate cycle: isocitrate lyase (Spot 81). We identified two enzymes involved in gluconeogenesis: enolase 1 (Spot 74) and Triose phosphate isomerase (Spot 84). Finally, we identified the mitochondrial outer membrane protein porin 1 (Spot 68) and a group of proteins of the stress

response pathway: glutaredoxin (Spot 70) and the mitochondrial peroxiredoxin (Spot 88).

3.4 Validation of proteomic results

In order to validate proteomic results, the amount of GAPDH, 3-phosphoglycerate kinase (Pkg1p), and porin 1 (Por1p) was evaluated by Western blot analysis (Fig. 4A). In line with the proteomic results (Fig. 4B), the amount of GAPDH and Pkg1p in the *sco1*-Δ yeast strain on SCG was similar to that of *sco1*-Δ yeast and wt-BY4741 on SCD. In fact, in *sco1*-Δ yeast on SCG, the GAPDH amount was 2.7-fold higher and the Pkg1p amount was 1.8-fold higher than in wt-BY4741 on SCG. Moreover, on SCG, this mutant displayed a decrease of the Por1p level compared to both the wild type on SCG (fourfold lower) and to *sco1*-Δ yeast and wt-BY4741 on SCD (threefold and 3.8-fold, respectively).

Furthermore, the enzyme activity of enolase 2 and isocitrate lyase was assayed (Fig. 5). On SCG, the increase of enolase expression level found in *sco1*-Δ mutant is associated with a twofold increased enzyme activity compared to wt-BY4741 on SCG. Concerning the isocitrate lyase, on SCG, *sco1*-Δ cells displayed an enzyme activity similar to that of wt-BY4741 and *sco1*-Δ cells on SCD while it resulted 28-fold lower compared to the wt-BY4741 strain on SCG in agreement with the 2-DE results.

The proteomic data pointed out that on SCG, *sco1*-Δ mutant strain displayed an increase in the expression level of some fermentative enzymes such as pyruvate decarboxylase 1 and alcohol dehydrogenase 1. To confirm these results, we assayed ethanol production during both mid-exponential phase and after 24 h of growth on SCG. We observed a higher fermentative capacity of the *sco1*-Δ mutant cells compared to the wt-BY4741 strain (Fig. 6A). The amount of ethanol production in *sco1*-Δ mutant cells during mid-exponential growth was 23-fold higher than in the wt-BY4741 strain. After 24 h, this difference was more evident; with an ethanol output in mutant strain 54 times that of control strain. These data suggested that yeast cells reconfigure their metabolism from respiration to fermentation as response to the lack of *SCO1* gene. To support this hypothesis, we also evaluated the oxygen consumption in this experimental condition. On SCG, *sco1*-Δ mutant cells were nonrespiring since no oxygen consumption was observed (Fig. 6B). To clarify whether the ethanol is produced as a result of fermentation of the 0.1% glucose present in the media or whether a part of glycerol is utilized as substrate, we evaluated the glucose and glycerol consumption on SCG for 24 h (Fig. 6C and D). We found that in *sco1*-Δ mutant, the glucose consumption rate was higher than in wt-BY4741 since glucose was exhausted after 8 h instead of 10 h observed for wild type. On the contrary, in *sco1*-Δ mutant, no glycerol consumption was detected after 24 h of growth. These experiments confirmed that *sco1*-Δ mutant has nonrespiring phenotype on SCG and that ethanol is

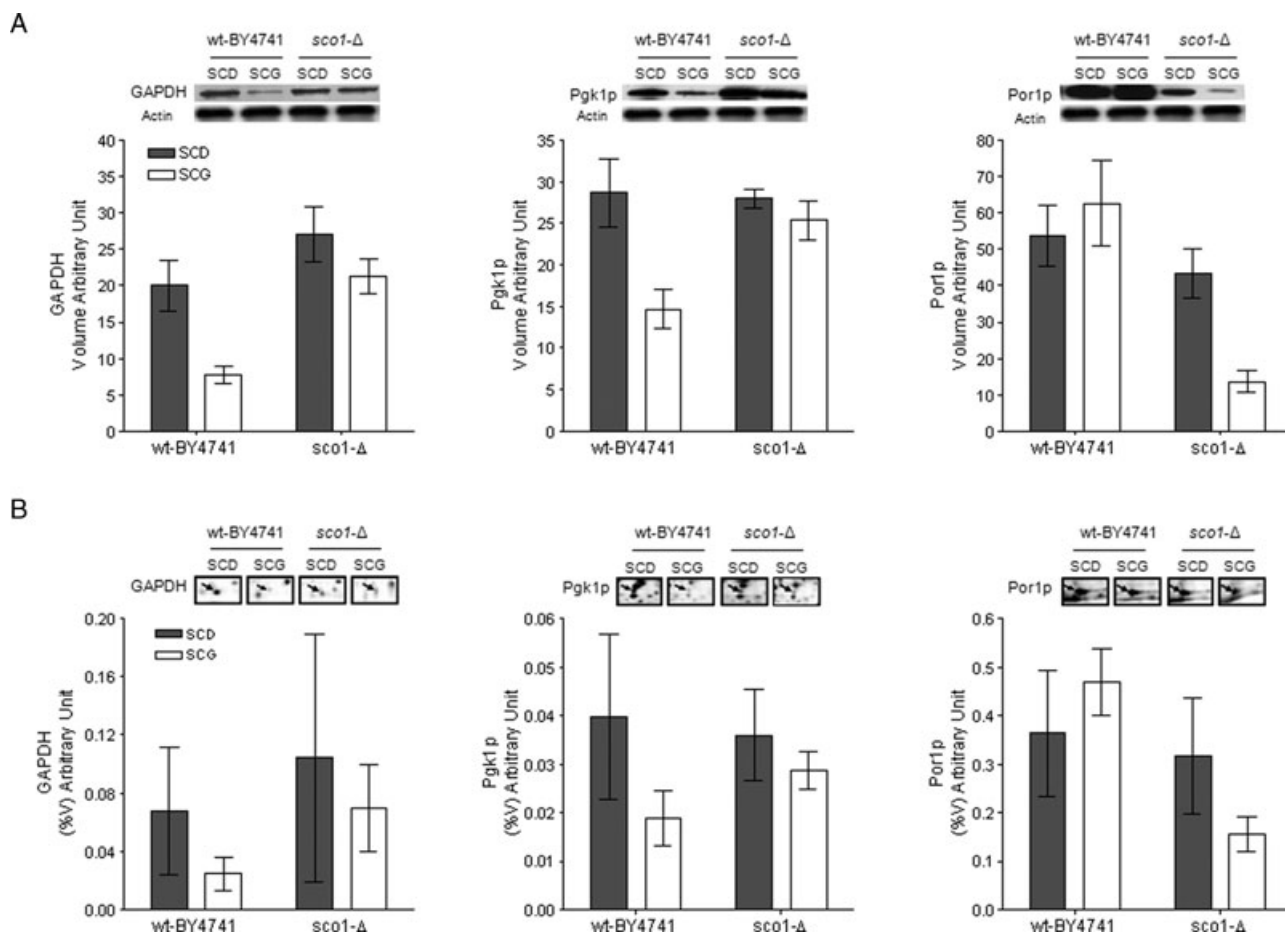


Figure 4. (A) Representative Western blot images and relative densitometric bar graphs of GAPDH (glyceraldehyde-3-phosphate dehydrogenase 1), phosphoglycerate kinase (Pgk1p), porin 1 (Por1p) for wt-BY4741, and *sco1*-Δ yeast strains grown on SCD (closed bars) and on SCG (open bars). Actin was used as protein loading control. Data represent mean and standard deviation obtained from three independent experiments. (B) Representative 2-DE images and relative densitometric bar graphs of GAPDH spot (n.13), Pgk1p spot (6), and Por1p spot (68) for wt-BY4741 and *sco1*-Δ yeast strains cultured on SCD (closed bars) and SCG (open bars).

produced by fermentation of the 0.1% glucose present in the medium.

4 Discussion

In this study, we investigated the effect of *SCO1* deletion on *S. cerevisiae* metabolism by comparing the proteome of *sco1*-Δ yeast strain with that of wt-BY4741 during mid-exponential phase on both fermentable and nonfermentable carbon sources. We used wt-BY4741 as control strain since it has been demonstrated, using complementation tests, that the kanMX deletion cassette was without significant effect on *sco1*-Δ phenotype [33].

The proteomic analysis pointed out differentially expressed protein belonging to several functional categories: energy metabolism, C-compound and carbohydrate metabolism, oxygen and reactive oxygen species metabolism, protein and amino acid biosynthesis, protein translocation, folding and

transport of metabolites. To present our results, we used a cluster analysis that groups similarly responsive protein spots. Clusters 2 and 4 include proteins whose expression profiles depend on growth conditions instead of *SCO1* deletion. On the other hand, clusters 1, 3, and 5 are the most relevant groups of differentially expressed protein spots, representing proteins that could be affected directly or indirectly by *SCO1* gene deletion. Clusters 1, 3, and 5 show that *SCO1* mutation has consequences on the proteome only during respiratory growth condition. In fact, on SCG, the *sco1*-Δ mutant proteome profile displays a high degree of similarity to that of wild type and *sco1*-Δ on SCD. In particular, *sco1*-Δ mutant cells grown on SCG showed a down-regulation of some gluconeogenic and oxidative metabolism-related proteins and an increase of some glycolytic and fermentative enzymes (cluster 1). The differences observed in the levels of some TCA enzymes and of some COX subunits in the *sco1*-Δ mutant could reflect mitochondrial dysfunction (cluster 5). This is probably connected to the role of Sco1p in COX

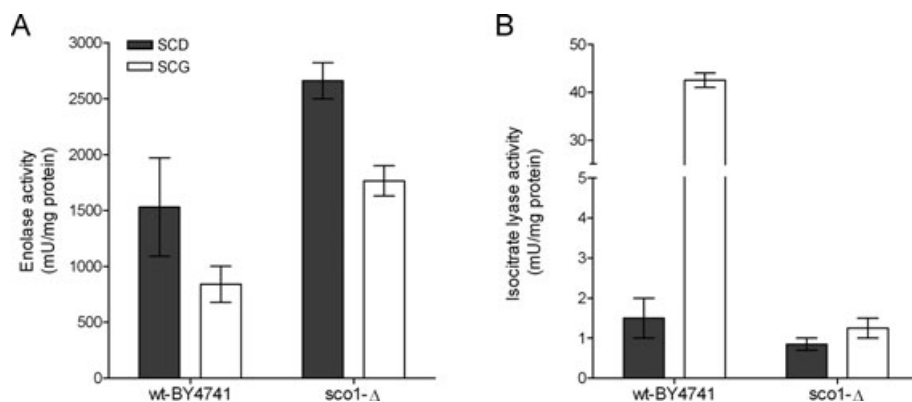


Figure 5. Specific activity of enolase (A) and isocitrate lyase (B) for wt-BY4741 and *sco1*-Δ mutant strain cultured on SCD (closed bars) and on SCG (open bars). Data represent mean and standard deviation obtained from two independent experiments.

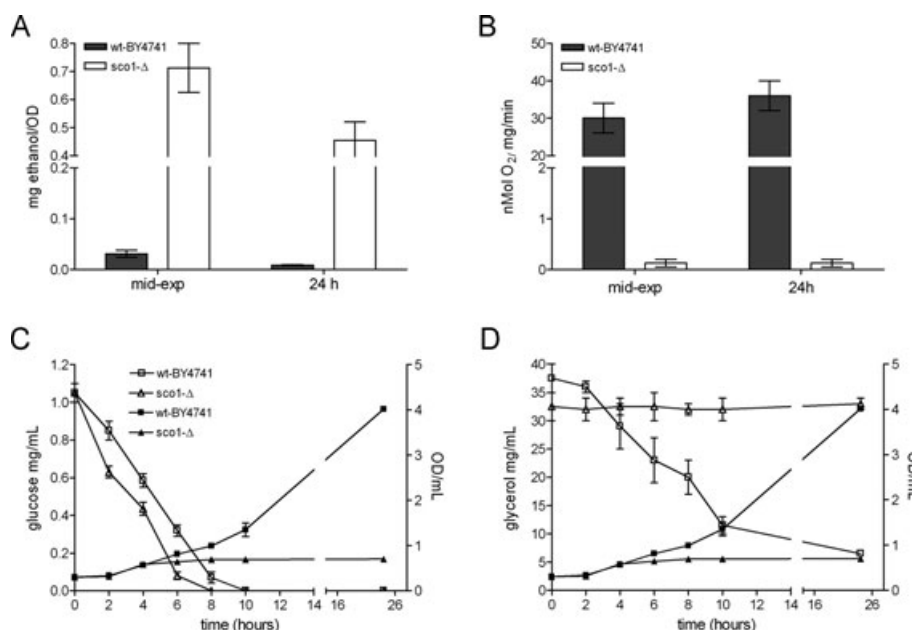


Figure 6. Analytical determinants. Ethanol production (A) and oxygen consumption (B) in wt-BY4741 (closed bars) and *sco1*-Δ mutant strain (open bars) on SCG medium at mid-exponential phase and after 24 h of growth. Glucose (C) and glycerol (D) consumption in wt-BY4741 (□) and *sco1*-Δ mutant strain (Δ) on SCG medium for 24 h. Data represent mean and standard deviation obtained from three independent experiments.

assembly and hence in respiratory chain activity. Moreover, the reduced level of several subunits of the ATP synthase complex could justify growth defects on nonfermentable carbon sources. Deletion of *ATP* genes leads to a “petite” phenotype that is slow-growing and unable to survive on nonfermentable carbon sources [34]. In cluster 3, which includes protein spots over-expressed in *sco1*-Δ on SCG, we found Asc1p, ortholog of the mammalian protein RACK1, which has broad array of functions. Yeast Asc1p and RACK1 are core 40S ribosomal proteins and are implicated in translational control [35]. Moreover, Asc1p functions as G-protein beta subunit of Gpa2p involved in the Ras2/cAMP pathway. In this regard, the increase of Asc1p expression level could be linked to the ATP synthase defect observed in the *sco1*-Δ mutant strain grown on glycerol. This hypothesis is based on a previous study that has shown an unusual relationship between Ras growth-regulatory pathway and mitochondrial energy transduction. In particular, T. Mubachi [36] demonstrated that RAS2/ASC1 expression suppresses the growth

defect caused by *ATP1-2* mutation. The proteomic results pointed out that the lack of *SCO1* leads to mitochondrial dysfunction and to an increase of some glycolytic and fermentative enzymes. These findings imply that *sco1*-Δ mutant cells to overcome the absence of a functional mitochondrial respiratory chain and to maintain ATP supplies may adapt their metabolism by repressing the expression of genes involved in the respiratory metabolism and conversely activating fermentative genes, regardless of the carbon source. In these regards, the *sco1*-Δ mutant showed an increase in enolase enzymatic activity and ethanol production. The ethanol is produced as a result of fermentation of the 0.1% glucose present in SCG media since we demonstrated the inability of the mutant to consume glycerol and thus to grow on medium containing only this carbon source. The claim that yeast cells reconfigure their metabolism from respiration to fermentation was also supported by the fact that on SCG *sco1*-Δ cells do not consume oxygen. Since *sco1*-Δ mutant is able to metabolize only 0.1% glucose, despite the activation of some

fermentative enzymes, it showed a reduced growth phenotype on SCG.

Our results suggest that the *sco1-Δ* mutant cells displayed on SCG a similar defective response as respiratory-deficient petite cells. Recently, it has been shown that petite mutants are defective in up-regulation of genes involved in utilization of nonfermentable carbon source, suggesting the involvement of mitochondrial function in glucose repression [37]. It should be notice that several reports have provided evidence that compromised mitochondria, such as in respiratory-deficient petite cells, lead to a compensatory genome response that has been termed “retrograde” response [38–40]. This is a pathway of communication from mitochondria to the nucleus whereby the expression of some nuclear genes is altered in cells with mitochondrial dysfunction. The main feature of this response is the activation of alternative pathways that compensate for respiratory-deficient state [41]. Because *sco1-Δ* mutant cells displayed a similar defective response as respiratory-deficient petite cells, we hypothesized that the loss of *SCO1* gene can lead to the retrograde response activation. These findings are in line with our previous paper on *SCO* mutants [14]. In fact, we found in *sco1-Δ* yeast mitochondrial proteome an increase in the expression level of Cit1p, an enzyme of the TCA cycle that is usually up-regulated in the retrograde response. However, apart from Cit1p, we did not find any other protein involved in the retrograde response. Thus, the possible retrograde response activation is worthy of further investigation.

We can conclude that in yeast cells grown on nonfermentable carbon sources, the deletion of *SCO1* gene seems to cause a metabolic switch (from respiration to fermentation) to overcome the absence of a functional mitochondrial respiratory chain and to maintain ATP supplies. Future studies should further investigate the effect of *SCO1* deletion on yeast metabolic pathways evaluating the activity of key enzymes during growth on fermentable and nonfermentable carbon sources and examining how genes known to be regulated by the retrograde response are regulated in wt-BY4741 and *sco1-Δ* mutant cells.

This work was supported by the FIRB grant “Italian Human ProteomeNet” (BRN07BMCT_013), from Italian Ministry of University and Scientific Research to L.B.

The authors have declared no conflict of interest.

5 References

- [1] Arnesano, F., Banci, L., Bertini, I., Martinelli, M., Ortholog search of proteins involved in copper delivery to cytochrome c oxidase and functional analysis of paralogs and gene neighbors by genomic context. *J. Proteome Res.* 2005, 4, 63–70.
- [2] Papadopoulou, L. C., Sue, C. M., Davidson, M. M., Tanji, K. et al., Fatal infantile cardioencephalomyopathy with COX deficiency and mutations in *SCO2*, a COX assembly gene. *Nat. Genet.* 1999, 23, 333–337.
- [3] Capaldi, R. A., Structure and function of cytochrome c oxidase. *Annu. Rev. Biochem.* 1990, 59, 569–596.
- [4] Poyton, R. O., Goehring, B., Droste, M., Sevarino, K. A. et al., Cytochrome-c oxidase from *Saccharomyces cerevisiae*. *Methods Enzymol.* 1995, 260, 97–116.
- [5] Tsukihara, T., Aoyama, H., Yamashita, E., Tomizaki, T. et al., Structures of metal sites of oxidized bovine heart cytochrome c oxidase at 2.8 Å. *Science* 1995, 269, 1069–1074.
- [6] Carr, H. S., Winge, D. R., Assembly of cytochrome c oxidase within the mitochondrion. *Acc. Chem. Res.* 2003, 36, 309–316.
- [7] Barrientos, A., Barros, M. H., Valnot, I., Rötig, A. et al., Cytochrome oxidase in health and disease. *Gene* 2002, 286, 53–63.
- [8] Tzagoloff, A., Dieckmann, C.L., PET genes of *Saccharomyces cerevisiae*. *Microbiol. Rev.* 1990, 54, 211–225.
- [9] Glerum, D. M., Shtanko, A., Tzagoloff, A., Characterization of COX17, a yeast gene involved in copper metabolism and assembly of cytochrome oxidase. *J. Biol. Chem.* 1996, 271, 14504–14509.
- [10] Glerum, D. M., Shtanko, A., Tzagoloff, A., *SCO1* and *SCO2* act as high copy suppressors of a mitochondrial copper recruitment defect in *Saccharomyces cerevisiae*. *J. Biol. Chem.* 1996, 271, 20531–20535.
- [11] Horng, Y. C., Cobine, P. A., Maxfield, A. B., Carr, H. S. et al., Specific copper transfer from the Cox17 metallochaperone to both Sco1 and Cox11 in the assembly of yeast cytochrome c oxidase. *J. Biol. Chem.* 2004, 279, 35334–35340.
- [12] Lode, A., Kuschel, M., Paret, C., Rödel, G., Mitochondrial copper metabolism in yeast: interaction between Sco1p and Cox2p. *FEBS Lett.* 2000, 485, 19–24.
- [13] Lode, A., Paret, C., Rödel, G., Molecular characterization of *Saccharomyces cerevisiae* Sco2p reveals a high degree of redundancy with Sco1p. *Yeast* 2002, 19, 909–922.
- [14] Gamberi, T., Magherini, F., Borro, M., Gentile, G. et al., Novel insights into phenotype and mitochondrial proteome of yeast mutants lacking proteins Sco1p or Sco2p. *Mitochondrion* 2009, 9, 103–114.
- [15] Leary, S. C., Kaufman, B. A., Pellicchia, G., Guercin, G. H. et al., Human *SCO1* and *SCO2* have independent, cooperative functions in copper delivery to cytochrome c oxidase. *Hum. Mol. Genet.* 2004, 13, 1839–1848.
- [16] Valnot, I., Osmond, S., Gigarel, N., Mehaye, B. et al., Mutations of the *SCO1* gene in mitochondrial cytochrome c oxidase deficiency with neonatal-onset hepatic failure and encephalopathy. *Am. J. Hum. Genet.* 2000, 67, 1104–1109.
- [17] Jaksch, M., Ogilvie, I., Yao, J., Kortenhaus, G. et al., Mutations in *SCO2* are associated with a distinct form of hypertrophic cardiomyopathy and cytochrome c oxidase deficiency. *Hum. Mol. Genet.* 2000, 9, 795–801.
- [18] Jaksch, M., Horvath, R., Horn, N., Auer, D. P. et al., Homozygosity (E140K) in *SCO2* causes delayed infantile onset of cardiomyopathy and neuropathy. *Neurology* 2001, 57, 1440–1446.

- [19] Horng, Y. C., Leary, S. C., Cobine, P. A., Young, F. B. et al., Human Sco1 and Sco2 function as copper-binding proteins. *J. Biol. Chem.* 2005, **280**, 34113–34122.
- [20] Bjellqvist, B., Pasquali, C., Ravier, F., Sanchez, J.-C. et al., A nonlinear wide-range immobilized pH gradient for two-dimensional electrophoresis and its definition in a relevant pH scale. *Electrophoresis* 1993, **14**, 1357–1365.
- [21] Görg, A., Postel, W., Günther, S., The current state of two-dimensional electrophoresis with immobilized pH gradients. *Electrophoresis* 1988, **9**, 531–546.
- [22] Hochstrasser, D. F., Harrington, M. G., Hochstrasser, A. C., Miller, M. J., Merrill, C. R., Methods for increasing the resolution of two-dimensional protein electrophoresis. *Anal. Biochem.* 1988, **173**, 424–435.
- [23] Oakley, B. R., Kirsch, D. R., Morris, N. R., A simplified ultrasensitive silverstain for detecting proteins in polyacrilamide gels. *Anal. Biochem.* 1980, **105**, 361–363.
- [24] Hellman, U., Wernstedt, C., Genez, J., Heldin, C. H., Improvement of an “in-gel” digestion procedure for the micropreparation of internal protein fragments for amino acid sequencing. *Anal. Biochem.* 1995, **224**, 451–455.
- [25] Soskic, V., Gorlach, M., Poznanovic, S., Boehmer, F. D. et al., Functional proteomics analysis of signal transduction pathways of the platelet-derived growth factor beta receptor. *Biochemistry* 1999, **38**, 1757–1764.
- [26] Meiring, H. D., van der Heeft, E., ten Hove, G. J., de Jong, A. P. J. M., Nanoscale LC-MS(n) technical design and applications to peptide and protein analysis. *J. Sep. Sci.* 2002, **25**, 557–568.
- [27] Brasma, A., Vilo, J., Gene expression data analysis. *FEBS Lett.* 2000, **480**, 17–24.
- [28] Giachetti, E., Pinzauti, G., Bonaccorsi, R., Vanni, P., Isocitrate lyase: characterization of its true substrate and the role of magnesium ion. *Eur. J. Biochem.* 1988, **172**, 85–91.
- [29] Bergmeyer, H. U., *Methods in Enzymatic Analysis*, Vol. II, 2nd ed., 1974, 449 p.
- [30] Dickinson, E. K., Adams, D. L., Schon, E. A., and Glerum, D. M., A human SCO2 mutation helps define the role of Sco1p in the cytochrome oxidase assembly pathway. *J. Biol. Chem.* 2000, **275**, 26780–26785.
- [31] Thevelein, J. M., Fermentable sugars and intracellular acidification as specific activators of the RAS-adenylate cyclase signalling pathway in yeast: the relationship to nutrient-induced cell cycle control. *Mol. Microbiol.* 1991, **5**, 1301–1307.
- [32] Rolland, F., Winderickx, J., Thevelein, J. M., Glucose-sensing and -signalling mechanisms in yeast. *FEMS Yeast Res.* 2002, **2**, 183–201.
- [33] Khalimonchuk, O., Bird, A., Winge, D. R., Evidence for a pro-oxidant intermediate in the assembly of cytochrome oxidase. *J. Biol. Chem.* 2007, **282**, 17442–17449.
- [34] Takeda, M., Chen, W. J., Saltzgaber, J., Douglas, M. G., Nuclear genes encoding the yeast mitochondrial ATPase complex. Analysis of ATP1 coding the F1-ATPase alpha-subunit and its assembly. *J. Biol. Chem.* 1986, **261**, 15126–15133.
- [35] Gerbasi, V. R., Weaver, C. M., Hill, S., Friedman, D. B. et al., Yeast Asc1p and mammalian RACK1 are functionally orthologous core 40S ribosomal proteins that repress gene expression. *Mol. Cell. Biol.* 2004, **24**, 8276–8287.
- [36] Mabuchi, T., Ichimura, Y., Takeda, M., Douglas, M. G., ASC1/RAS2 suppresses the growth defect on glycerol caused by the atp1-2 mutation in the yeast *Saccharomyces cerevisiae*. *J. Biol. Chem.* 2000, **275**, 10492–10497.
- [37] Kitagaki, H., Cowart, L. A., Matmati, N., Montefusco, D. et al., ISC1-dependent metabolic adaptation reveals an indispensable role for mitochondria in induction of nuclear genes during the diauxic shift in *Saccharomyces cerevisiae*. *J. Biol. Chem.* 2009, **17**, 10818–10830.
- [38] Epstein, C. B., Waddle, J. A., Hale, W., IV, Dave, V. et al., Genome-wide responses to mitochondrial dysfunction. *Mol. Biol. Cell.* 2001, **12**, 297–308.
- [39] Butow, R. A., Avadhani, N. G., Mitochondrial signaling: the retrograde response. *Mol. Cell* 2004, **14**, 1–15.
- [40] Jazwinski, S. M., Rtg2 protein: at the nexus of yeast longevity and aging. *FEMS Yeast Res.* 2005, **5**, 1253–1259.
- [41] Liu, Z., Butow, R. A., A transcriptional switch in the expression of yeast tricarboxylic acid cycle genes in response to a reduction or loss of respiratory function. *Yeast* 1999, **15**, 1377–1391.